HYbriD Resonant Acoustics (HYDRA)

*Amgad R. Rezk, James K. Tan, and Leslie Y. Yeo**

A longstanding convention in acoustomicrofluidic manipulation—a consequence of wholesale adoption from decades long application of surface acoustic waves (SAWs) in electronics and telecommunications—has been to employ pure SAWs by eliminating wave reflections and bulk resonances in single crystal piezoelectric substrates with the assumption that this provides the most efficient way to actuate fluid flow at microscale dimensions. Despite its many advantages, particularly for delivering next generation macromolecular-based therapeutics, the limitation of SAW devices, however, lies in the input power it can sustain, thus constraining the nebulisation rates that can be generated, which has, among other things, severely hampered its practical adoption in pulmonary drug administration to date. Here, we unravel, for piezoelectric devices with electrode configurations such as interdigital transducers that permit the generation of surface (Rayleigh) waves, the existence of, what we term, a surface reflected bulk wave (SRBW) that has yet to be explicated, and show, quite counter-intuitively, that it is possible to obtain an order-of-magnitude improvement in microfluidic manipulation efficiency through this unique combination of surface and bulk waves without increasing complexity or cost.

Since the 1950s, high frequency (HF) and very high frequency (VHF) surface acoustic waves (SAWs; nanometer amplitude Rayleigh electromechanical waves that propagate along and are confined to the surface of a piezoelectric substrate) between 10 MHz to several GHz have been extensively used primarily in the telecommunications industry for signal filtering and processing.[1] Today, it is not uncommon to find several SAW filter devices in mobile phones. These devices, in which interdigital transducer (IDT) electrodes are patterned on a single crystal piezoelectric substrate—typically lithium niobate—to generate the SAW, are designed specifically to eliminate spurious and bulk resonances through the substrate thickness which could interfere with the SAW.

One way in which this is done is to deliberately rotate the crystal, and, as such, almost all SAW filter devices employ a 128° *Y*-axis rotated, *X*-axis propagating single crystal lithium niobate cut (128YX LN).[2] Additionally, the thickness of the substrate h is designed to be substantially larger than the SAW wavelength λ_{SAW} to avoid wave leakage and reflection through the thickness of the substrate given that the SAW penetration depth varies inversely with the SAW resonant frequency f; in other words, the vibrational energy of the SAW is locally confined within a region along the surface of the substrate with a characteristic thickness that is typically of order $\lambda_{SAW} = c_{SAW}/f$, c_{SAW} being the Rayleigh SAW phase velocity.[3] As the thick (relative to λ_{SAW}) 128YX LN substrate is assumed to provide the best SAW piezoelectric coupling and hence the most efficient generation of the SAWs, this same material and large relative thickness has been used to date for microfluidic manipulation[4–10] for point-of-care diagnostic, drug delivery, and other applications.[11–20]

This use of pure SAWs, while opening up a myriad of possibilities in microfluidics, may however not always be the most efficient way to actuate fluid flow at the microscale. As but one example, the nebulization rates with SAW nebulization has to date been limited to 0.2–0.4 mL min^{-1},[21–24] frustrating efforts to translate an otherwise attractive and potentially powerful technology for pulmonary drug administration into clinical practice given its many advantages, such as the ability to generate aerosol sizes that are optimal for deep lung deposition[21] and the ability to deliver next generation therapeutic molecules (e.g., proteins, peptides, and nucleic acids[25]) without degradation. Further increasing the input power and hence the surface vibration amplitude in the attempt to obtain higher nebulization rates is not possible given that there exists a maximum power loading before the device fails. This is because the increase in the concentration of energy along the substrate surface as the input power is intensified gives rise to a large temperature gradient across this localized region of thickness λ_{SAW}, which given the pyroelectricity of 128YX LN, leads to singular electric fields particularly at the device's edges that promote local defect propagation and ultimately device failure.

In what follows, we demonstrate that it is not only possible to harness and efficiently utilize the bulk waves that leak from the SAW through the entire thickness of the substrate that all SAW-related work in 128YX LN to date has attempted to suppress but also show that these bulk waves can be uniquely exploited in combination with surface waves to drive extremely efficient microscale manipulation without further device cost or complexity. The latter is, in fact, quite counterintuitive given that bulk waves (e.g., Lamb waves), while capable of driving microfluidic flows,[26,27] have long been regarded to be an order-of-magnitude less efficient than its SAW counterpart. In addition, these plate waves, whose vibration extends through the entire substrate thickness, are limited to resonant frequencies of several MHz at most (unless very thin substrates are used, although this leads to a drastic compromise in their durability, especially when large mechanical strains are required for fluid actuation), leading to relatively large wavelengths (>1 mm), which are incompatible for microfluidic particle/cell manipulation.[28,29]

The different device configurations tested are shown by the schematics in **Figure 1**, from which it can be seen that the key design parameter is the ratio between the substrate thickness

Dr. A. R. Rezk, J. K. Tan, Prof. L. Y. Yeo
Micro/Nanophysics Research Laboratory
RMIT University
Melbourne, VIC 3000, Australia
E-mail: leslie.yeo@rmit.edu.au

DOI: 10.1002/adma.201504861

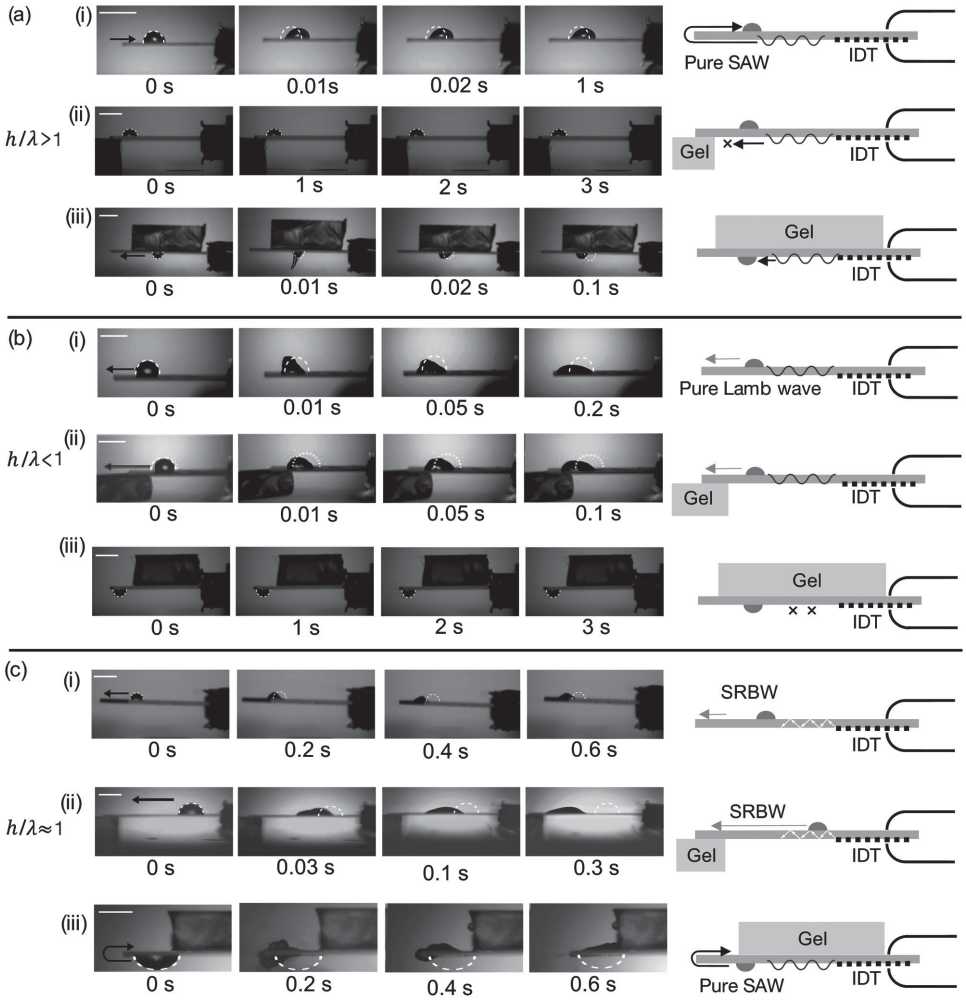

Figure 1. Time series images showing the translation of a sessile drop under a) a pure SAW ($h/\lambda > 1$), b) a pure antisymmetric Lamb wave ($h/\lambda < 1$), and c) an SRBW ($h/\lambda \approx 1$). The dotted lines indicate the initial positions of the drop at $t = 0$ whereas the schematics on the right depict the device and drop configurations (i) in the absence of an absorption gel, (ii) with the gel placed at the edge on the underside of the device, and (iii) with the gel placed on the top face of the device. All scale bars denote a length of 5 mm.

h and the acoustic wavelength λ, set by the pitch of the fingers that comprises the IDT electrodes (specifically, four times the finger width and gap). We achieve the various asymptotic cases here by maintaining h constant throughout and altering the resonant frequency of the device f and hence λ. Devices with h = 500 µm are fabricated by patterning 40 IDT finger pairs comprising 10 nm Cr and 1.5 µm Al with 3.9 mm aperture widths on a 128YX double-sided polished LN substrate (Roditi Ltd., London, UK) using standard photolithography. The acoustic wave is then generated by applying a sinusoidal electrical input at the resonant frequency to the IDTs with a signal generator (SML01, Rhode & Schwarz, North Ryde, NSW, Australia) and amplifier (LYZ-22+, Mini Circuits, Brooklyn, NY, USA), and characterized using laser Doppler vibrometry (LDV; UHF-120; Polytec PI, Waldbronn, Germany) scans. Deionized water at room temperature was used as the test fluid.

The conventional SAW device (Figure 1a) is therefore the case when $h/\lambda > 1$ (or more strictly, $h/\lambda > 3$), i.e., when the frequency is relatively large, such that the acoustic wave is confined to the surface. In our experiments, we employ f = 79.8 ± 0.1 MHz (the variation arising from slight differences in the IDT patterns from device to device that arose during fabrication) and λ = 50 µm such that h/λ = 10; it should be noted that the devices in all cases have been flipped such that the underside of the substrate constitutes the surface on which the IDTs that generate the SAW are patterned. In this configuration, the SAW energy, being confined within the penetration depth adjacent to the underside surface on which the SAW is generated, rapidly decays over a lengthscale exp ($-\beta z$) through the thickness of the device[3] (β being the attenuation coefficient over which the SAW decays in the solid in the vertical z direction) such that it is completely attenuated long before it reaches the top side of the substrate. In other words, no vibration on the top face exists due to leakage of the SAW energy through the thickness of the substrate, as verified from the LDV scans in **Figure 2**b. Instead, the SAW on the underside surface propagates to the edge (since there are no reflector IDTs) where it partially reflects (edge reflections of up to 70%

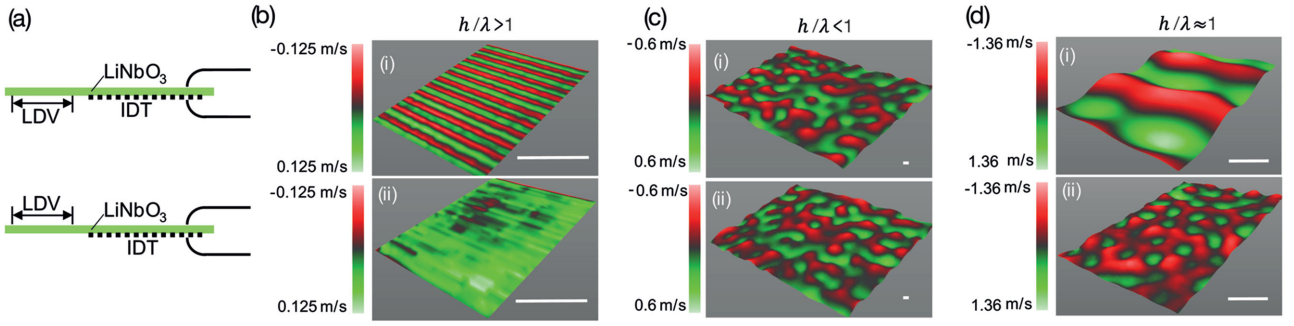

Figure 2. Acoustic wave characterization using laser Doppler vibrometry (LDV). a) Scans are taken on both the underside of the device on which the IDTs are fabricated (top row) as well as on the top face of the device (bottom row), as illustrated in the schematic. b) Pure SAW case ($h/\lambda > 1$) wherein (i) the SAW is generated on the underside of the device on which the IDTs are located and (ii) the SAW appears to be almost completely attenuated when it wraps around the edge of the device onto the top face. c) Pure Lamb wave case ($h/\lambda < 1$) in which the antisymmetric plate wave exists throughout the entire thickness of the substrate, (i,ii) manifesting as a quasi-2D wave pattern on both faces due to edge reflections. d) Hybrid surface and bulk wave case, i.e., HYDRA ($h/\lambda \approx 1$), in which (i) surface and (ii) reflected bulk waves are observed on the underside and the top face of the device, respectively; the quasi-2D wave pattern that appears in (ii) is due to the combination of wave reflection within the substrate and the interaction with the SAW which wraps around the edge from the underside to the top face of the device. In all cases, the input power applied to the device is 4 W. All scale bars denote a length of 250 μm.

have been typically reported in similar devices[30,31]); the rest of the SAW however continues to propagate around the edge of the device onto the top side, although its energy attenuates on the substrate surface along its propagation direction x as exp $(-\alpha x)$, wherein α is the longitudinal attenuation coefficient of the SAW in an unbounded fluid, i.e., either in air or in liquid if one is present on the substrate.[32] This effect is observed in Figure 1a–i where a millimeter dimension sessile drop, placed on the top face of the device, is observed to be transported due to the SAW which has wrapped around the edges from the underside of the device; that a drop with height much greater than λ_{SAW} translates in the SAW propagation direction due to Eckart streaming is well known.[33–35] When gel (Geltec Ltd., Yokohama, Japan) is however placed on the underside of the substrate to absorb the SAW, the translation (as well as vibration) of the drop appears to be suppressed (Figure 1a–ii). In contrast, when the gel is placed on the top face (on which any other waves other than the SAW that wraps around the edge from the underside should be nonexistent since $h/\lambda > 1$), a drop placed on the underside was observed, as expected, to translate along the SAW propagation direction (Figure 1a–iii); jetting effects were also observed since the SAW had not attenuated as much on the underside compared to the case when it has propagated further distances when it wraps around onto the topside.

On the other hand, when $h/\lambda < 1$, bulk (fundamental symmetric and antisymmetric Lamb) waves can be generated through the thickness of the substrate, as has previously been demonstrated in 128YX LN.[27,36] Exciting the fundamental antisymmetric frequency of the Lamb wave at 3.0 ± 0.1 MHz (λ = 1000 μm and hence h/λ = 0.5), as shown in Figure 1b, results in the entire substrate thickness vibrating in-phase with similar displacement amplitudes (Figure 2c). A drop placed on either face of the device is therefore displaced along the wave propagation direction; this is shown when the drop is on the top face in Figure 1b–i although similar behavior is observed when the drop is placed on the underside on which the IDTs are patterned (not shown). The placement of gel at the edge on the underside of the device only acts to absorb the bulk wave locally; a drop placed on the top face is therefore observed to still translate along the propagation direction of the wave that is left undisturbed in the rest of the substrate through its entire thickness (Figure 1b–ii). Placing the gel across a large proportion of the top face however completely damps the vibration, not just along the top surface but also through its entire thickness, such that the displacement of the drop is completely suppressed (Figure 1b–iii); such sensitivity to fluid loading or mounting of the device is a widely known disadvantage in the practical use of these plate waves.

To examine the intermediate asymptotic case when $h/\lambda \approx 1$, we choose an operating frequency of 14.2 ± 0.1 MHz corresponding to λ = 280 μm and hence h/λ = 1.8, which lies in the approximate range between 1 and 3 where symmetric and antisymmetric Lamb waves, which possess phase velocities higher and lower than that of the SAW, respectively, asymptote toward the SAW phase velocity c_{SAW}.[37] In other words, the choice of h/λ is deliberate such that it lies within the threshold at which the wave converges from a bulk Lamb wave to a Rayleigh surface wave. While it has long been known that fundamental Lamb waves (regime I) eventually converge into Rayleigh surface waves (i.e., SAWs; regime III) as h/λ increases, as illustrated in the dispersion characteristics in **Figure 3**a, the intermediate regime where this transition from bulk to surface waves takes place (regime II) has yet to be explored.

In particular, the energy associated with the SAW, which propagates along the underside of the substrate, leaks through the entire thickness of the device in this transition regime and is therefore no longer completely attenuated at the top face of the substrate as in the case of the pure SAW in Figure 1a where $h/\lambda > 1$. In contrast, the SAW that propagates on the underside on which the IDTs are located (Figure 2d–i) leaks in phase through the substrate thickness and manifests as a travelling surface wave along the top side (Figure 2d–ii), in what we term as a surface reflected bulk wave (SRBW; Figure 1c) while reflecting off this side to constructively recombine with the SAW on the underside. To date, the individual identity of such waves, to our best knowledge, has yet to be distinguished

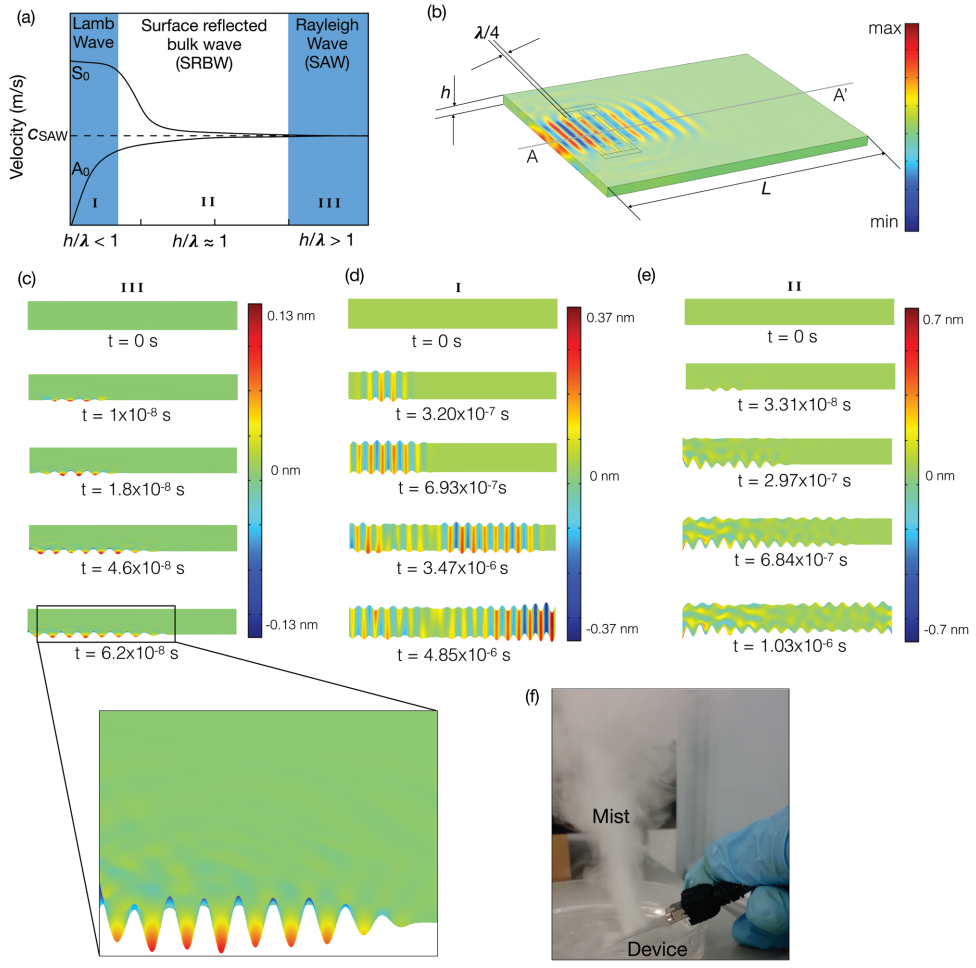

Figure 3. a) Sketch of the wave dispersion curves showing the fundamental antisymmetric (A_0) and symmetric (S_0) modes. An intermediate asymptotic region (regime II; $h/\lambda \approx 1$) exists as the Lamb waves (regime I) are gradually superseded by Rayleigh surface waves (regime III) with increasing h/λ. b–e) Numerical results across a 2D section (A–A') through the thickness of the 128YX LN substrate (note that the substrate in (b) has been reversed for ease of visualization; the electrodes used to generate the waves are placed on the underside of the device in (c–e)), obtained from a 3D time-dependent finite element simulation for three cases: (c) an 80 MHz device ($h/\lambda = 10$; regime III) in which we observe a SAW is generated and confined along the underside of the device on which the IDTs are placed; d) a 3 MHz device ($h/\lambda = 0.5$; regime I) in which we observe a classical Lamb wave is generated (regime I); and e) a 14 MHz device ($h/\lambda = 1.8$; HYDRA) in which the SAW that is initially generated on the underside of the device leaks through its thickness and reflects off the top face to form an SRBW (regime II). f) The latter configuration (HYDRA) can be exploited to produce large nebulization rates up to 8 mL min^{-1} when the edge of the device is immersed in a liquid reservoir.

and classified, let alone examined, having merely been simply referred to generically as bulk acoustic waves (BAWs) together with all the other bulk waves that exist.[38] In other words, no attempt has been made to date to elucidate the nature of these waves let alone to utilize them.

We note that these waves are not simply higher harmonic Lamb waves, as confirmed by calculations of the wave velocity from the wavelength, set by the IDT dimension, and the resonant frequency, measured from the insertion loss parameter (Figure S1, Supporting Information), which are significantly lower than those for higher order resonances which are known to possess much larger values (above 6000 m s^{-1}) for h/λ values up to 2.[37] We also note that the SRBW, although akin in appearance to surface skimming bulk waves (SSBWs), possesses very different characteristics: the SSBW "skims" beneath the surface by propagating within and through the bulk of the material rather than along the top and bottom surfaces of the substrate; moreover, the SSBW is a horizontally polarized shear wave, with no vertical out-of-plane component unlike the SRBW.

In contrast to the case of the pure SAW in Figure 1a–i and not unlike the case of the Lamb wave in Figure 1b–i, a drop on the top face of the device is observed to translate in the opposite direction (Figure 1c–i); we note that the translation still occurs in the direction of the wave propagation, although that of the SRBW propagation and not of the SAW propagation, which still exists and wraps around the edge of the device from its underside but is weak compared to the SRBW having attenuated considerably along its long propagation path. If the SAW on the underside of the device is suppressed by absorbing it with the gel, we observe the drop to translate faster since the SAW no longer wraps around the edge of the device to the top

face to oppose the SRBW (Figure 1c–ii); parenthetically, we also note the different spreading characteristics of the drop[35,39–41] given that the SRBW is different in nature to the Rayleigh surface wave. Unlike the case of the Lamb wave in Figure 1b–iii, however, absorbing the wave with the gel on the top side of the device only suppresses the SRBW on this face but not the SAW on the underside. As such, a drop placed on the underside in this configuration is seen to translate along the SAW propagation direction, and to even climb around the edge of the device to its top face along with the SAW propagation (Figure 1c–iii). These observations, together with the LDV scans in Figure 2d, verifies the distinction of the SRBW from the Lamb wave shown in Figure 2c.

The distinction between the SAW in Figure 1a, the Lamb wave in Figure 1b, and the SRBW in Figure 1c is further corroborated via numerical simulations. Here, we employ a finite element analysis that incorporates a 3D time-dependent piezoelectric model for the substrate (including the crystal rotation and constants relevant to the 128YX LN cut) patterned with three electrode pairs to which a time-periodic potential is applied (Figure 3b); free boundary conditions are imposed along all faces. A multigrid mesh model is used with ≈5 million nodes, with convergence being achieved when the mass and momentum residuals decreased below 10^{-6}. The substrate thickness is set to be constant (h = 500 μm) in all simulations, while the electrode finger width and gap, and subsequently the wavelength λ, is varied.

Unlike the case for the pure SAW (Figure 3c) or the fundamental antisymmetric Lamb wave (Figure 3d), it can be seen from the simulation results that the SRBW, which arises for the case $h/\lambda = 1.8$ as shown in Figure 3e, is not simply a higher harmonic Lamb wave, thus corroborating our earlier hypothesis and wave velocity calculations. Instead, the SAW that is initially generated on the underside of the device (see, e.g., the result at $t = 3.31 \times 10^{-8}$ s) is observed to gradually leak through the thickness of the substrate ($t = 2.97 \times 10^{-7}$ s), reflecting off the top face and coupling back to the SAW ($t = 6.84 \times 10^{-7}$ s), which eventually reaches the edge of the device and wraps around to the top face to interact with the SRBW ($t = 1.03 \times 10^{-6}$ s). Additionally, we also note that the reflected bulk wave, i.e., the SRBW, constructively recombines with the SAW that, in turn, leaks to further strengthen the SRBW; these multiple reflections then set up a positive reinforcement cycle such that the displacement amplitude of the SRBW is enhanced. We therefore note the marked contrast between the SRBW in Figure 3e with the usual antisymmetric Lamb wave pattern obtained in Figure 3d for the 3 MHz case in which $h/\lambda = 0.5$.

The LDV scans in Figure 2 (a sketch of the location at which the scans are acquired is shown in Figure 2a) reveal a far greater vibrational velocity for this hybrid surface and bulk wave combination ($h/\lambda \approx 1$)—about one order of magnitude (Figure 2d) over that obtained with the pure surface wave ($h/\lambda > 1$) configuration (Figure 2b) and more than two times that obtained with the pure bulk (Lamb) wave ($h/\lambda < 1$) configuration (Figure 2c)—and suggests that greater gains in acoustic excitation efficiency can be gleaned using this setup, despite the prevailing assumption that surface waves are generally more efficient than bulk waves, at least where acoustomicrofluidic actuation is concerned.[5,15–20]

To demonstrate this, we choose a microfluidic application which requires by far the highest power density—nebulization. Pure SAW devices are typically limited to nebulization rates up to ≈0.4 mL min^{-1}[21–24] due to device failure as a result of the large thermal gradients and hence voltages that exceed the threshold value for dielectric breakdown in the material that arise locally on the substrate surface. In contrast, the hybrid combination of the surface and bulk waves, i.e., the SRBW and the SAW in the configuration shown in Figure 1c–i, is able to sustain larger increases in the input power as the acoustic energy and hence the thermal gradients are no longer confined to the acoustic penetration depth, but are distributed through the entire substrate. Together with the substantially higher vibrational velocities, achieved through mutual reinforcement via multiple reflection and constructive recombination events, it can be seen that these HYbriD Resonance Acoustic (HYDRA) devices, while retaining a similar physical mechanism for nebulization due to substrate acceleration driven interfacial deformation and its inherent advantages,[21,22] are able to enhance the nebulization rate by more than an order of magnitude compared to pure SAW devices and two to three orders of magnitude compared to pure Lamb wave devices up to 8 mL min^{-1} (Figure 3f; see also Table S1, Supporting Information). This therefore circumvents a major technological limitation faced by SAW microfluidic nebulization devices that constitutes the dominant hurdle in their practical deployment for pulmonary drug delivery: a highly inadequate nebulization rate which prevents sufficient drug from being delivered in a practical inhalation period through a portable miniature consumer drug delivery platform. Additionally, we anticipate the efficiency gains with the HYDRA configuration could lead to improved performance for other drop and microchannel transport and manipulation schemes in microfluidic devices (an example of the complex streaming flow generated by the SRBW in a sessile drop is shown in Figure S2, Supporting Information), therefore potentially opening up various applications in acoustofluidics not possible to date.

In summary, we show, contrary to longstanding conventional acceptance and without introducing further cost or complexity, that it is not only acceptable but also expedient to retain bulk waves through the thickness of a single crystal piezoelectric substrate—surface reflected bulk waves—which, when employed in concert with surface acoustic waves through judicious design, can lead to significantly improved performance for microfluidic manipulation, and especially nebulization where sufficiently large aerosol delivery rates are crucial if the device is to be practically useful for inhalation therapy. It is thus expected that these first HYbriD Resonance Acoustic devices will not only circumvent the severe limitations that have prevented the adoption of surface acoustic wave microfluidic nebulization devices for pulmonary drug delivery of next generation therapeutics but also open up new wide ranging possibilities for high power acoustofluidics across large-scale nanoparticle synthesis, therapeutic encapsulation, and crystallization.

Supporting Information

Supporting Information is available from the Wiley Online Library or from the author.

Acknowledgements

L.Y.Y. was funded through an Australian Research Council (ARC) Future Fellowship (FT130100672) as well as Discovery Project grant DP140100805. A.R.R. is grateful for an RMIT University Vice-Chancellor's Research Fellowship.

Received: October 2, 2015
Revised: November 13, 2015
Published online: January 7, 2016

[1] R. White, F. Voltmer, *Appl. Phys. Lett.* **1965**, *7*, 314.
[2] K. Shibayama, K. Yamanouchi, H. Sato, T. Meguro, *Proc. IEEE* **1976**, *64*, 595.
[3] E. Soczkiewicz, *Nondestr. Test. Eval.* **1997**, *13*, 113.
[4] T. Frommelt, M. Kostur, M. Wenzel-Schäfer, P. Talkner, P. Hänggi, A. Wixforth, *Phys. Rev. Lett.* **2008**, *100*, 034502.
[5] J. Friend, L. Y. Yeo, *Rev. Mod. Phys.* **2011**, *83*, 647.
[6] Y. Bourquin, R. Wilson, Y. Zhang, J. Reboud, J. M. Cooper, *Adv. Mater.* **2011**, *23*, 1458.
[7] Y. J. Liu, X. Ding, S.-C. S. Lin, J. Shi, I.-K. Chiang, T. J. Huang, *Adv. Mater.* **2011**, *23*, 1656.
[8] R. J. Shilton, M. Travagliati, F. Beltram, M. Cecchini, *Adv. Mater.* **2014**, *26*, 4941.
[9] S. Collignon, J. Friend, L. Y. Yeo, *Lab Chip* **2015**, *15*, 1942.
[10] R. J. Shilton, V. Mattoli, M. Travagliati, M. Agostini, A. Desii, F. Beltram, M. Cecchini, *Adv. Funct. Mater.* **2015**, *25*, 5895.
[11] S. Schneider, S. Nuschele, A. Wixforth, C. Gorzelanny, A. Alexander-Katz, R. Netz, M. Schneider, *Proc. Natl. Acad. Sci. USA* **2007**, *104*, 7899.
[12] S. R. Heron, R. Wilson, S. A. Shaffer, D. R. Goodlett, J. M. Cooper, *Anal. Chem.* **2010**, *82*, 3985.
[13] X. Ding, S.-C. S. Lin, B. Kiraly, H. Yue, S. Li, I.-K. Chiang, J. Shi, S. J. Benkovic, T. J. Huang, *Proc. Natl. Acad. Sci. USA* **2012**, *109*, 11105.
[14] J. Reboud, Y. Bourquin, R. Wilson, G. S. Pall, M. Jiwaji, A. R. Pitt, A. Graham, A. P. Waters, J. M. Cooper, *Proc. Natl. Acad. Sci. USA* **2012**, *109*, 15162.
[15] X. Ding, P. Li, S.-C. S. Lin, Z. S. Stratton, N. Nama, F. Guo, D. Slotcavage, X. Mao, J. Shi, F. Costanzo, T. J. Huang, *Lab Chip* **2013**, *13*, 3626.
[16] Y. Bourquin, A. Syed, J. Reboud, L. C. Ranford-Cartwright, M. P. Barrett, J. M. Cooper, *Angew. Chem., Int. Ed.* **2013**, *53*, 5587.
[17] L. Y. Yeo, J. R. Friend, *Annu. Rev. Fluid Mech.* **2014**, *46*, 379.
[18] G. Destgeer, S. Im, B. H. Ha, J. H. Jung, M. A. Ansari, H. J. Sung, *Appl. Phys. Lett.* **2014**, *104*, 023506.
[19] G. Destgeer, H. J. Sung, *Lab Chip* **2015**, *15*, 2722.
[20] G. Destgeer, B. H. Ha, J. Park, J. H. Jung, A. Alazzam, H. J. Sung, *Anal. Chem.* **2015**, *87*, 4627.
[21] A. Qi, J. R. Friend, L. Y. Yeo, D. A. Morton, M. P. McIntosh, L. Spiccia, *Lab Chip* **2009**, *9*, 2184.
[22] D. J. Collins, O. Manor, A. Winkler, H. Schmidt, J. R. Friend, L. Y. Yeo, *Phys. Rev. E* **2012**, *86*, 056312.
[23] A. Rajapaksa, A. Qi, L. Y. Yeo, R. Coppel, J. R. Friend, *Lab Chip* **2014**, *14*, 1858.
[24] A. Winkler, S. Harazim, S. Menzel, H. Schmidt, *Lab Chip* **2015**, *15*, 3793.
[25] A. E. Rajapaksa, J. J. Ho, A. Qi, R. Bischof, T.-H. Nguyen, M. Tate, D. Piedrafita, M. P. McIntosh, L. Y. Yeo, E. Meeusen, R. L. Coppel, J. R. Friend, *Respir. Res.* **2014**, *15*, 60.
[26] W. Liang, G. Lindner, *J. Appl. Phys.* **2013**, *114*, 044501.
[27] A. R. Rezk, J. R. Friend, L. Y. Yeo, *Lab Chip* **2014**, *14*, 1802.
[28] T. Laurell, F. Petersson, A. Nilsson, *Chem. Soc. Rev.* **2007**, *36*, 492.
[29] M. Wiklund, B. Unfelt, *Methods Mol. Biol.* **2012**, *853*, 177.
[30] A. K. Gautesen, *Wave Motion* **1987**, *9*, 51.
[31] R. D. Gregory, I. Gladwell, *J. Elasticity* **1983**, *13*, 185.
[32] R. Arzt, E. Salzmann, K. Dransfeld, *Appl. Phys. Lett.* **1967**, *10*, 165.
[33] C. Eckart, *Phys. Rev.* **1948**, *73*, 373.
[34] P. Brunet, J. Eggers, R. D. Deegan, *Eur. Phys. J. Spec. Top.* **2009**, *166*, 11.
[35] A. R. Rezk, O. Manor, J. R. Friend, L. Y. Yeo, *Nat. Commun.* **2012**, *3*, 1167.
[36] A. R. Rezk, L. Y. Yeo, J. R. Friend, *Langmuir* **2014**, *30*, 11243.
[37] Y. Jin, S. G. Joshi, *IEEE Trans. Ultrason., Ferroelectr., Freq. Control* **1996**, *43*, 491.
[38] C. Campbell, *Surface Acoustic Wave Devices for Mobile and Wireless Communications*, Academic, San Diego, CA, **1998**.
[39] X. Noblin, A. Buguin, F. Brochard-Wyart, *Phys. Rev. Lett.* **2005**, *94*, 166102.
[40] P. Brunet, M. Baudoin, O. Bou Matar, F. Zoueshtiagh, *Phys. Rev. E* **2010**, *81*, 036315.
[41] O. Manor, M. Dentry, J. R. Friend, L. Y. Yeo, *Soft Matter* **2011**, *7*, 7976.